Valorization of construction and demolition (C&D) and industrial wastes through alkali activation

Dimitra Zaharaki, Michalis Galetakis, Kostas Komnitsas *

School of Mineral Resources Engineering, Technical University of Crete, University Campus, 73100 Chania, Greece

HIGHLIGHTS

- Waste co-valorization is in line with zero-waste and circular economy principles.
- Molar ratios in raw materials, such as SiO_2/Al_2O_3 and SiO_2/CaO affect process.
- Final products exhibit good strength and thermal properties.

ARTICLE INFO

ABSTRACT

In the present experimental study, the valorization of construction and demolition (C&D) and industrial wastes, namely ferronickel slag and red mud, through alkali activation is investigated. Specimens were produced by mixing various proportions of the raw materials with NaOH and sodium silicate solutions. The paste was cast in cubic metal moulds with an edge of 5 cm, cured at 80 °C for 24 h and then aged for 7 days at room temperature. The produced specimens were subjected to compressive strength testing. The effect of the molarity of the activating solution, the mineralogy of the raw materials and the ratios of SiO_2/Al_2O_3 and $SiO_2/(Al_2O_3 + CaO)$ on the compressive strength of the final products was investigated. Also, the effect of high temperature heating (400–800 °C) on the structural integrity of the produced specimens was assessed. The use of analytical techniques, namely X-ray diffraction, Thermogravimetric Analysis, Fourier Transform Infrared Spectroscopy and Scanning Electron Microscopy provided insights on the morphology, structure and thermal resistance of the produced specimens.

© 2016 Elsevier Ltd. All rights reserved.

1. Introduction

Alkali activation of aluminosilicates at relatively low temperature results in the production of cementitious materials, usually called geopolymers or inorganic polymers, which are characterized by a partially or fully amorphous polymeric structure consisting of Si–O–Al bonds. Their properties such as high early strength, chemical and high temperature resistance, depend mainly on the mineralogy of the raw materials as well as on the strength of the alkaline activator used [1,2]. Other parameters affecting their structure are the curing process and the aging period [3,4].

Alkali activated materials have attracted considerable attention in the last three decades due to their properties that render them suitable as alternative binders in the construction industry, as fire-/corrosion resistant materials or as matrices for the encapsulation of hazardous elements. Recent research efforts have mainly focused on the valorization of a wide variety of wastes and the production of materials with appropriate physico-chemical, mechanical and thermal properties [5–10].

The reactivity of raw materials during alkali activation is mainly related to the percentage of their amorphous content [11]. The mechanisms involved in this process have been elucidated to a certain extent by the use of several analytical techniques including Scanning Electron Microscopy (SEM), Fourier Transform Infrared Spectroscopy (FTIR), X-ray Diffraction (XRD), Nuclear Magnetic Resonance (NMR) Spectroscopy and Thermogravimetric Analysis (TG) [12–16].

The alkali activation potential of industrial wastes such as fly ash from thermal power plants, slag from the steel industry and red mud from alumina production, has been extensively investigated. Fly ash has been considered for the production of elements with suitable physico-chemical and mechanical properties that can be used in the construction industry or for immobilization of toxic

elements [17–21]. High or low calcium slags have been alkali activated for the production of materials that can be used in various industrial applications [22–27]. Other recent studies have shown that wastes such as fly ash, granulated blast furnace slag (GBFS) and calcium carbide residue can be alkali activated and used as binders to replace Ordinary Portland Cement (OPC) for the production of "green" concrete as well as for the production of other construction elements with lower carbon footprint [28–31]. The alkali activation potential of red mud mixed with other industrial wastes has been also exploited for the production of bricks, tiles and fire resistant construction materials [32,33].

On the other hand, the alkali activation potential of C&D wastes still remains a challenge and a rather limited number of studies have been carried out so far. More specifically, Allahverdi and Kani [34,35] produced geopolymer cement using waste bricks and concrete in different mixing ratios. They found that waste bricks exhibited better alkali activation potential compared to concrete. Ahmari et al. [36] produced geopolymeric binder from mixtures of waste concrete and fly ash. When high alkaline NaOH solutions were used (10 M) the compressive strength of the final products reached almost 30 MPa. Reig et al. [37] investigated the properties and microstructure of alkali-activated cement pastes and mortars produced from red clay brick waste. They optimised the type and concentration of alkali activator to produce mortars with compressive strength up to 50 MPa after 7 days of curing at 65 °C. Sun et al. [38] produced geopolymer-type materials by activating waste ceramics. The synthesized products exhibited very good thermal stability and compressive strength of over 75 MPa. Pathak et al. [39] investigated two types of C&W wastes, i.e. concrete powder and brick powder, to produce geopolymers. Calorimetric analysis showed that brick dust is more reactive than concrete waste and the final products exhibited maximum compressive strength over 10 MPa. It was deduced from their study that the physicomechanical properties of geopolymers obtained from these C&D waste components were comparable with those of other building materials. Zedan et al. [40] investigated the effect of mixing ceramic, red clay brick and concrete wastes with ground granulated blast furnace slag (GGBFS) on the properties of the produced alkali activated slag cement. It is mentioned that GGBFS has a much lower Fe_2O_3 and higher CaO content than the ferronickel slag used in this study.

All these studies prove that most components of C&D waste entail a noticeable alkali activation potential. This potential may be enhanced if specific ratios of components are mixed to adjust the mineralogical composition of the starting raw materials prior to alkali activation [41]. It has to be underlined that the European Commission has identified C&D wastes as a priority waste flow for reuse and highlighted the noticeable environmental benefits of their valorization (Directive 2008/98/EC) [42,43]. These benefits include among others reduction of the consumption of natural resources, minimization of the volume of wastes that will ultimately be landfilled and reduction of the emission of greenhouse gases (GHGs) [44–46].

The present experimental study aims to investigate the co-valorization of C&D and industrial wastes, namely ferronickel slag and red mud, through alkali activation and define the main factors that affect the properties of the produced materials. The proposed approach is in line with the "zero-waste" and "circular economy" principles of the European Commission and contributes to "closing the loop" of product lifecycles through greater recycling and reuse, while it brings maximum benefits for both the environment and the economy.

2. Experimental procedure

2.1. Materials

The raw materials used in the present study were:

(i) electric arc furnace slag from the "LARCO S.A" ferronickel plant in Larymna, prefecture of Lokris, central Greece,
(ii) C&D waste components i.e. tiles, bricks and concrete collected from various demolished buildings in the city of Chania, island of Crete, Greece and
(iii) red mud from "Aluminium of Greece", Agios Nikolaos plant, prefecture of Veotia, central Greece.

All materials were pulverized using a BICO Type UA pulveriser and a FRITSCH pulveriser and homogenized. Grain size analysis was determined using a Mastersizer S (Malvern Instruments) particle size analyser (Table 1). The chemical composition of the raw materials, as derived from an X-ray fluorescence energy dispersive spectrometer (XRF–EDS) Bruker-AXS S2 Range type, is presented in Table 2. Loss on ignition (LOI) was determined by heating each raw material at 1050 °C for 4 h.

2.2. Methodology

In the present study, raw materials were used after grinding in various mixtures. The % w/w of each raw material subjected to alkali activation as well as the codes of all specimens are presented in Table 3. The percentage of each raw material was selected by taking into account its mineralogical composition and previous studies carried out by the authors.

Raw materials were mixed under continuous stirring with the activating solution, which was prepared by dissolving NaOH anhydrous pellets (Sigma Aldrich) in distilled water and then adding sodium silicate solution (Na_2O = 7.5–8.5%, SiO_2 = 25.5–28.5%, Merck). The final solution was allowed to cool at room temperature for 24 h prior to use.

The required amount of NaOH pellets was dissolved in distilled water to obtain solution molarity 8, 10 or 12 M. The liquid/solid (L/S) ratio varied slightly between 0.27 and 0.33 in order to improve the flowability characteristics of the produced paste before casting. The fresh paste was cast in cubic metal moulds of 5 cm edge, which were vibrated for a few minutes to eliminate the presence of air voids in the reactive mass and improve the properties of the final specimens. The moulds remained at room temperature for 4 h to allow early initiation of reactions which favour the development of structural bonds and solidification of the paste. Then the specimens were demoulded and sealed in plastic bags to prevent fast evaporation of water during curing.

The specimens were then heated at 80 °C in a laboratory oven (ON-02G) for 24 h, allowed to cool and after aging at room temperature for 7 days were subjected to compressive strength testing using a MATEST C123N load frame. The thermal behaviour of the specimens was evaluated after heating at high temperature (400, 600 and 800 °C) for 1 h in a laboratory furnace N-8L Selecta; weight loss, volumetric shrinkage and porosity (using a Micromeritics AutoPore 9400 porosimeter) were also recorded. All tests and measurements were carried out in triplicate.

Table 1
Particle size (μm) of raw materials.

	Slag	Tiles	Bricks	Concrete	Red mud
Size (μm)	<120	<140	<140	<190	<76
d_{50} (μm)	12	14	7	10	4

Table 2
Chemical composition (%) of raw materials.

Material	Fe_2O_3	SiO_2	Al_2O_3	CaO	Na_2O	K_2O	MgO	TiO_2	Cr_2O_3	LOI	SUM
Slag	43.83	36.74	9.32	3.73	–	–	2.76	–	2.82	–	99.2
Tiles	5.39	70.54	9.80	8.78	–	1.37	4.46	0.77	–	–	101.1
Bricks	6.00	57.79	14.95	8.79	1.03	2.80	4.75	0.85	–	1.89	98.9
Concrete	0.75	5.81	1.49	65.42	0.57	1.26	4.21	0.03	–	21.59	101.1
Red mud	41.65	9.28	15.83	10.53	2.26	0.21	–	4.73	–	16.77	101.3

Table 3
% w/w of each raw material used for the production of each alkali activated specimen.

Code	Slag	Tiles	Bricks	Concrete	Red mud
S	100	–	–	–	–
T	–	100	–	–	–
B	–	–	100	–	–
C	–	–	–	100	–
R	–	–	–	–	100
50S-20T-20B-10C	50	20	20	10	–
25S-30T-30B-15C	25	30	30	15	–
50S-10T-10B-30C	50	10	10	30	–
90S-10R	90	–	–	–	10
80S-20R	80	–	–	–	20
70S-30R	70	–	–	–	30
60S-40R	60	–	–	–	40
50S-50R	50	–	–	–	50

XRD analysis of the raw materials and the produced specimens was performed using a Bruker AXS (D8 Advance type) diffractometer with Cu tube, scanning range from 4° to 70° 2θ, step 0.02° and measuring time 0.2 s/step. The qualitative analysis was assessed with the use of the DIFFRAC^{plus} EVA v. 2006 software and the Powder Diffraction File (PDF-2) database. TG analysis was carried out using a TGA-6/DTG Perkin Elmer differential thermogravimetric analyser (temperature measurement precision ±2 °C, microbalance sensitivity <5 μg). The experiments were carried out at atmospheric pressure under nitrogen atmosphere, with a flow rate of 100 mL/min and a heating rate of 10 °C/min. FTIR analysis was carried out using pellets produced after mixing a pulverized sample of each specimen with KBr at a ratio of 1:100 w/w, using a Perkin-Elmer Spectrum 1000 spectrometer (USA). SEM analysis was performed with a JEOL 6380LV scanning electron microscope equipped with an EDS INCA microanalysis system with low vacuum, pressure 30 Pa, voltage 20 kV and 10–12 mm working distance from the detector. Samples were mounted in resin and thin polished sections were prepared and used for SEM studies.

3. Results and discussion

3.1. Effect of activating solution molarity on compressive strength

Fig. 1 shows the compressive strength of the specimens produced by mixing ferronickel slag with C&D wastes in various percentages as a function of the molarity of the activating solution (8, 10 or 12 M NaOH); specimen codes are presented in Table 3. It also shows the indicative compressive strength of the control specimens (S, T, B and C) produced at 10 M NaOH, for comparison.

It is seen from Fig. 1 that the strength of alkali activated specimens is affected by the molarity of the activating solution. At 8 M NaOH the strength of the specimens for all mixing combinations tested is around 55 MPa, 30% lower than the strength of the control slag specimen S. When the molarity of the alkaline solution increases to 10 M NaOH a noticeable beneficial effect on the compressive strength for all specimens is shown. The highest values, around 76 MPa, are obtained for specimens which are produced
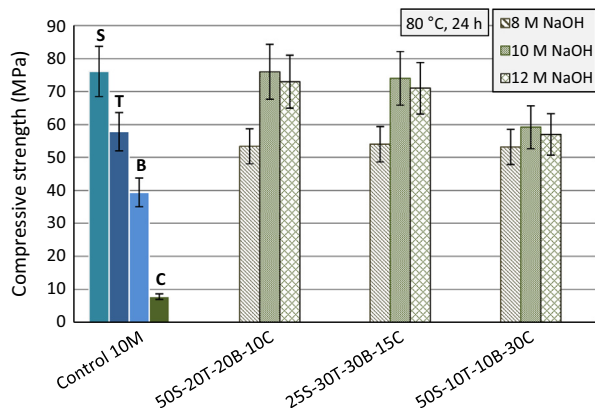
from raw material mixtures containing lower percentages of concrete, i.e. 10 and 15% w/w (specimens 50S-20T-20B-10C and 25S-30T-30B-15C, respectively). When the percentage of concrete increases to 30% w/w (specimen 50S-10T-10B-30C) the strength drops to just below 60 MPa. When the molarity increases to 12 M NaOH, the strength is slightly decreased compared to 10 M NaOH, by almost 4%, for all alkali activated combinations tested. This is maybe due to the presence of unreacted residual alkalis which makes solidification more slow and results in partial loss of strength. Lower molarity of NaOH (8 M) does not seem to provide the overall required alkalinity in the initial paste and thus less Si and Al ions are dissolved from the raw materials and participate in the formation of stronger bonds. It is thus deduced that the optimum NaOH molarity for alkali activation of slag and C&D waste components is 10 M.

Fig. 2 shows the compressive strength of slag-red mud specimens for various mixing ratios vs. the molarity of NaOH. It is shown from this figure that the optimum NaOH molarity is also 10 M, as discussed in Fig. 1. The compressive strength of the produced specimens decreases gradually when increased red mud addition percentages are used in the initial mixtures and reaches almost 40 MPa when the slag:red mud ratio is 1:1 (50S-50R specimen), which is still an acceptable value for several construction applications. By taking into account that red mud alone cannot be alkali activated, as indicated by the compressive strength of the control R specimen which is just 2.5 MPa, it is deduced that in order to obtain materials with adequate compressive strength that can be used in the construction industry, red mud should be mixed with other suitable raw materials that improve the properties of the initial mixture.

3.2. Effect of the molar ratios of oxides present in the initial paste

Table 4 shows the molar ratios of various oxides present in the initial paste, aiming to elucidate the role of the mineralogy of the raw materials during alkali activation. In this table the compressive strength of all specimens, including the control ones produced from slag, single components of C&D waste and red mud during alkali activation with 10 M NaOH are also presented for comparison.

First of all, it is seen that since slag, tiles and to a lesser degree bricks are successfully alkali activated, the compressive strength of the specimens produced using noticeable percentages of these raw materials is also high. On the other hand, it is shown that higher percentage of concrete and red mud in the initial paste results in decrease of the compressive strength.

It is known that specimens with high compressive strength are usually obtained when high SiO_2/Al_2O_3 molar ratios are present in the initial paste [41]; these ratios are for example 7.33 and 12.67 when only slag (S) or tiles (T) are alkali activated. High SiO_2/Al_2O_3
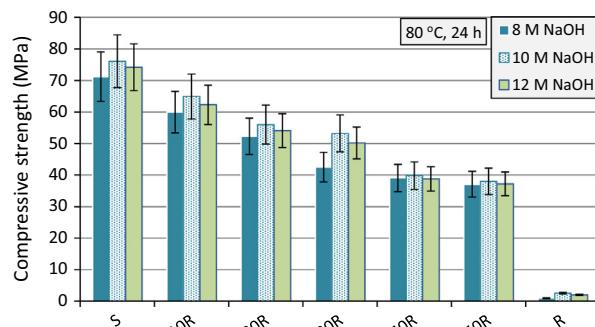

Fig. 1. Compressive strength of specimens produced by mixing slag with C&D wastes (error bars denote standard deviation of three specimens).

Fig. 2. Compressive strength of slag-red mud specimens as a function of NaOH molarity (error bars denote standard deviation of three specimens).

Table 4
Molar ratios of oxides present in the initial paste (10 M NaOH) and compressive strength of alkali activated products.

Code	$\frac{SiO_2}{Al_2O_3}$	$\frac{SiO_2}{CaO}$	$\frac{SiO_2}{(Al_2O_3+CaO)}$	$\frac{SiO_2}{(Al_2O_3+Fe_2O_3)}$	$\frac{H_2O}{(Na_2O+K_2O)}$	Strength (MPa)
S	7.33	8.97	4.03	1.68	8.30	76.1
T	12.67	7.76	4.81	9.38	9.03	57.8
B	6.84	6.38	3.30	5.44	8.32	39.4
C	9.86	0.12	0.12	7.47	6.62	7.8
R	1.33	1.10	0.60	0.50	8.11	2.5
50S-20T-20B-10C	8.5	3.62	2.54	3.18	6.89	76.0
25S-30T-30B-15C	8.86	2.95	2.21	4.54	6.10	74.1
50S-10T-10B-30C	8.26	1.38	1.18	2.67	6.96	59.2
90S-10R	6.26	7.04	3.31	1.55	7.80	65
80S-20R	5.44	5.76	2.80	1.43	7.42	56
70S-30R	4.74	4.77	2.38	1.32	7.16	53.2
60S-40R	4.07	3.93	2.00	1.19	6.84	39.8
50S-50R	3.53	7.20	1.70	1.08	6.66	38

molar ratios facilitate the formation of dense and strong Si–O–Al and Si–O–Si bonds.

When the SiO_2/Al_2O_3 ratio is very low, such as the one present in red mud paste (1.33), very few aluminosilicate bonds are formed and thus the final strength is also low (2.5 MPa for R specimen), as discussed in Section 3.4 and in other studies [47,48]. The very low strength of red mud specimens is also related to the low values of the ratios SiO_2/CaO and $SiO_2/(Al_2O_3 + CaO)$ as shown in Table 4 (1.10 and 0.60, respectively), due to the low SiO_2 content (9.28%) of red mud. Also, the $SiO_2/(Al_2O_3 + Fe_2O_3)$ molar ratio is very low, just 0.5 for the R paste. It is thus deduced that when both ratios SiO_2/Al_2O_3 and $SiO_2/(Al_2O_3 + Fe_2O_3)$ are low in the starting mixture the final compressive strength of the specimens will be low. When both these ratios increase the compressive strength also increases as also shown for all combinations of mixtures between slag and red mud (90S-10R to 50S-50R). When the $SiO_2/(Al_2O_3 + Fe_2O)$ ratio is low, specimens can only acquire high strength if the SiO_2/Al_2O_3 ratio is high, as shown for the S specimen.

Regarding concrete, it is deduced from Table 4 that SiO_2/Al_2O_3 and SiO_2/CaO are the critical ratios. Concrete has by far the lowest SiO_2 (5.81%) and Al_2O_3 (1.49%) and the highest CaO content, thus despite the fact that the SiO_2/Al_2O_3 ratio is high in the initial paste (9.86) both SiO_2/CaO and $SiO_2/(Al_2O_3 + CaO)$ ratios are extremely low (0.12), and since no alkali activation occurs to dissolve raw materials and generate Si and Al ions that result in the formation of aluminosilicate bonds, the compressive strength of the produced specimens is very low.

On the other hand, as Table 4 data shows concrete can be mixed with slag and other C&D components, up to 30% w/w in the starting mixture, and alkali activated without affecting noticeably the final strength of the produced specimens. This is due to the fact that both critical ratios, as mentioned earlier, are improved (specimens 50S-20T-20B-10C, 25S-30T-30B-15C and 50S-10T-10B-30C).

The ratio $H_2O/(Na_2O + K_2O)$ in the initial paste does not seem to affect the final compressive strength since it is high in all combinations of raw materials used. It only shows that adequate water was available in the reactive paste allowing the initiation of alkali activation reactions. Whether or not these reactions will progress and to which degree depends on the presence of appropriate percentages of the required mineralogical phases so that optimum ratios among SiO_2, Al_2O_3 and CaO are present, as discussed earlier, under the condition that sufficient concentration of alkali activator is used.

It has to be underlined though that apart from the above mentioned ratios, which indicate the alkali activation potential of specific raw materials, the strength of alkali activation solution

and the reactivity of the most important phases present in raw materials define the properties of the final products. It is known that the solubility of Si, Al, and Fe is very important [2,49]. It is also known that NaOH dissolves more Si and Al from raw materials compared to KOH [50]. The role of calcium is also important and the formation of C-S-H and C-A-S-H phases is also possible if the raw materials contain elevated calcium content, as in the case of recycled concrete and red mud. On the other hand, it has to be taken into account that the solubility of calcium decreases at elevated pH and results in the formation of unstable calcium hydroxide, which induces atmospheric carbonation and thus specimens with lower strength are obtained [51,52].

3.3. Thermal stability

Fig. 3 presents the compressive strength of selected specimens prepared from slag (S) as well as from mixtures of slag with C&D waste (25S-30T-30B-15C) or red mud (90S-10R, 50S-50R) and then subjected to high temperature heating at 400, 600 and 800 °C for one hour. The compressive strength of the control specimens, which were not subjected to high temperature heating, is also given for comparison.

It is shown that for all specimens strength decreases gradually when temperature increases from 400 to 800 °C. The best behaviour is shown for specimens S, prepared only from slag, and 25S-30T-30B-15C, prepared by mixing slag with C&D waste components; despite the fact that their strength decreases by almost 60% at 800 °C, it still remains at acceptable values for structural materials when subjected to thermal heating, close to 30 MPa. Thus, these materials may be used for passive fire protection in constructions, as also reported by Sakkas et al. [53]. It is also shown in Fig. 3 that the slag-red mud specimen 90S-10R which was produced from a starting mixture with higher slag content (90% w/w) also retains an acceptable strength value after heating at 800 °C (~20 MPa) which is much higher than the strength of 50S-50R specimen (~8 MPa), in which the slag to red mud weight ratio is 1:1.

The decrease in the compressive strength of specimens that were subjected to high temperature heating is mainly related to the increased weight loss and volumetric shrinkage that reach 11% and 8%, respectively. Also the decrease in porosity, which for example for specimen 50S-50R heated at 800 °C reaches 25%, is an important factor that affects the mechanical properties of the produced specimens since it is accompanied by the development of easily visible microcracks. The same behaviour has been also observed in one of our recent studies [41]. All these factors cause deterioration of the structural integrity of the specimens as a result of the partial decomposition of Si–O–Al and Si–O–Si bonds, as also discussed in other studies [54–58].
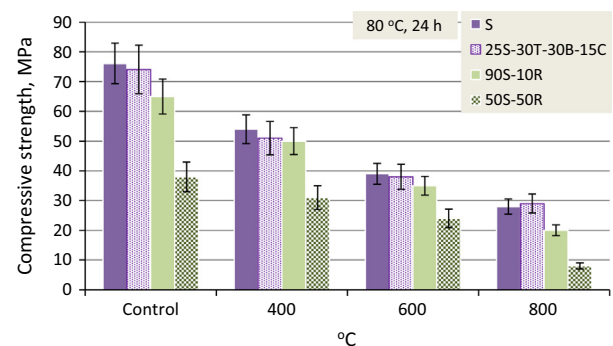

Fig. 3. Compressive strength of selected specimens subjected to high temperature heating (error bars denote standard deviation of three specimens).
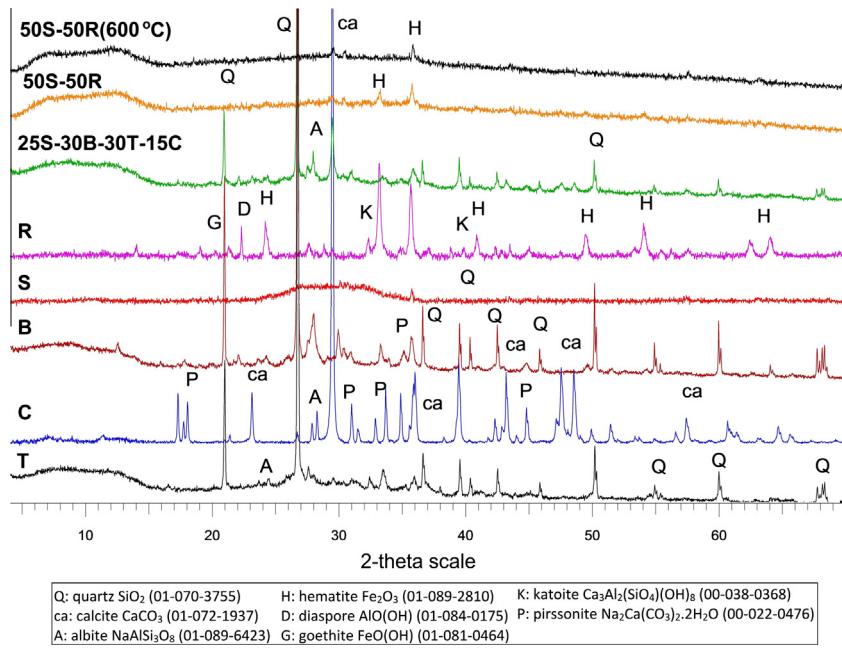
Fig. 4. XRD patterns of selected specimens produced from slag, C&D waste components and red mud (specimen codes are presented in Table 3).
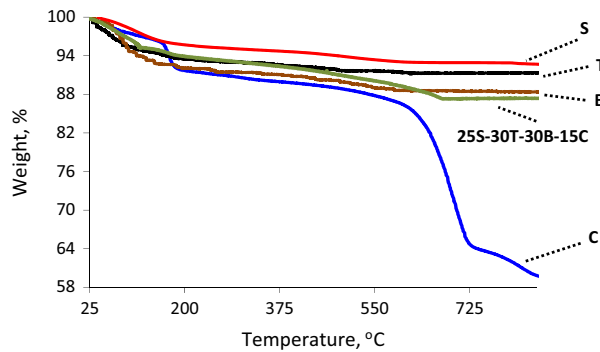

Fig. 5. TG curves of selected specimens produced from slag and C&D waste components (specimen codes are presented in Table 3).

3.4. Morphology of final products

Our previous studies show that the mineralogy of ferronickel slag is dominated by the presence of amorphous silicate or aluminosilicate phases exceeding 50% w/w. C&D waste components con-

Table 5
FTIR spectra band assignments.

Band number, cm^{-1}	Assignment
3440, 2950, 2340, 1830	H–O–H stretching and bending vibrations
1490, 1420, 880	Atmospheric carbonation, out of plane bending of CO_3
1050	Si–O stretching vibrations and Si–O–Si or Al–O–Si asymmetric stretching vibrations
710–460	In plane Si–O bending and Al–O linkages as well as bending Si–O–Si and O–Si–O vibrations

tain various crystalline phases such as quartz and calcite, while red mud consists mainly of hematite, goethite and diaspore [2,41].

Fig. 4 presents the XRD patterns of three selected specimens produced from mixtures of slag, C&D waste components and red mud as well as of the respective control specimens produced after alkaline activation with the use of 10 M NaOH. It is seen from this figure that all specimens consist of partially reacted or unreacted crystalline phases, such as quartz, calcite, hematite and albite, which were also present in the raw materials. The formation of
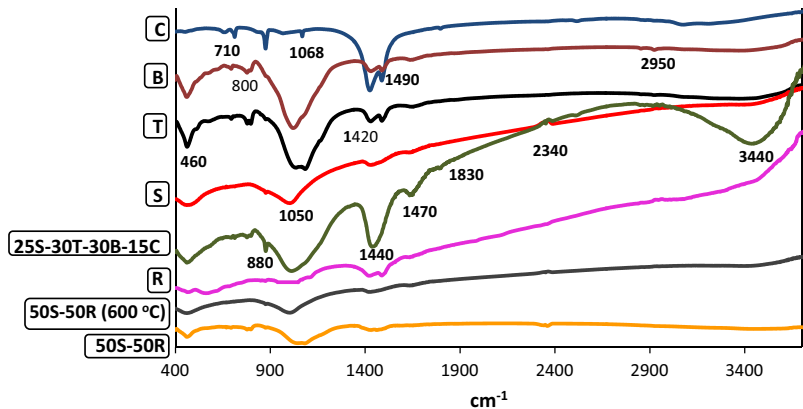

Fig. 6. FTIR spectra of selected specimens produced from slag, C&D waste components and red mud (specimen codes are presented in Table 3).

pirssonite, $(Na_2Ca(CO_3)_2 \cdot 2H_2O)$, in specimens T, C and B is due to atmospheric carbonation.

It is also seen in Fig. 4 that slag-based specimens (S) which acquire the highest compressive strength are characterized by certain degree of amorphicity [59]. In specimens produced from C&D components which also exhibit quite high degree of amorphicity,

such as B and T, and acquire also high strength, the peaks between 27° and 42° 2-theta become broader. On the other hand, limited amorphicity is shown in the XRD patterns of C and R specimens which acquire low strength; in these specimens only unreacted crystalline phases are present. It is also shown that no significant changes are present in the XRD pattern of 50S-50R specimen
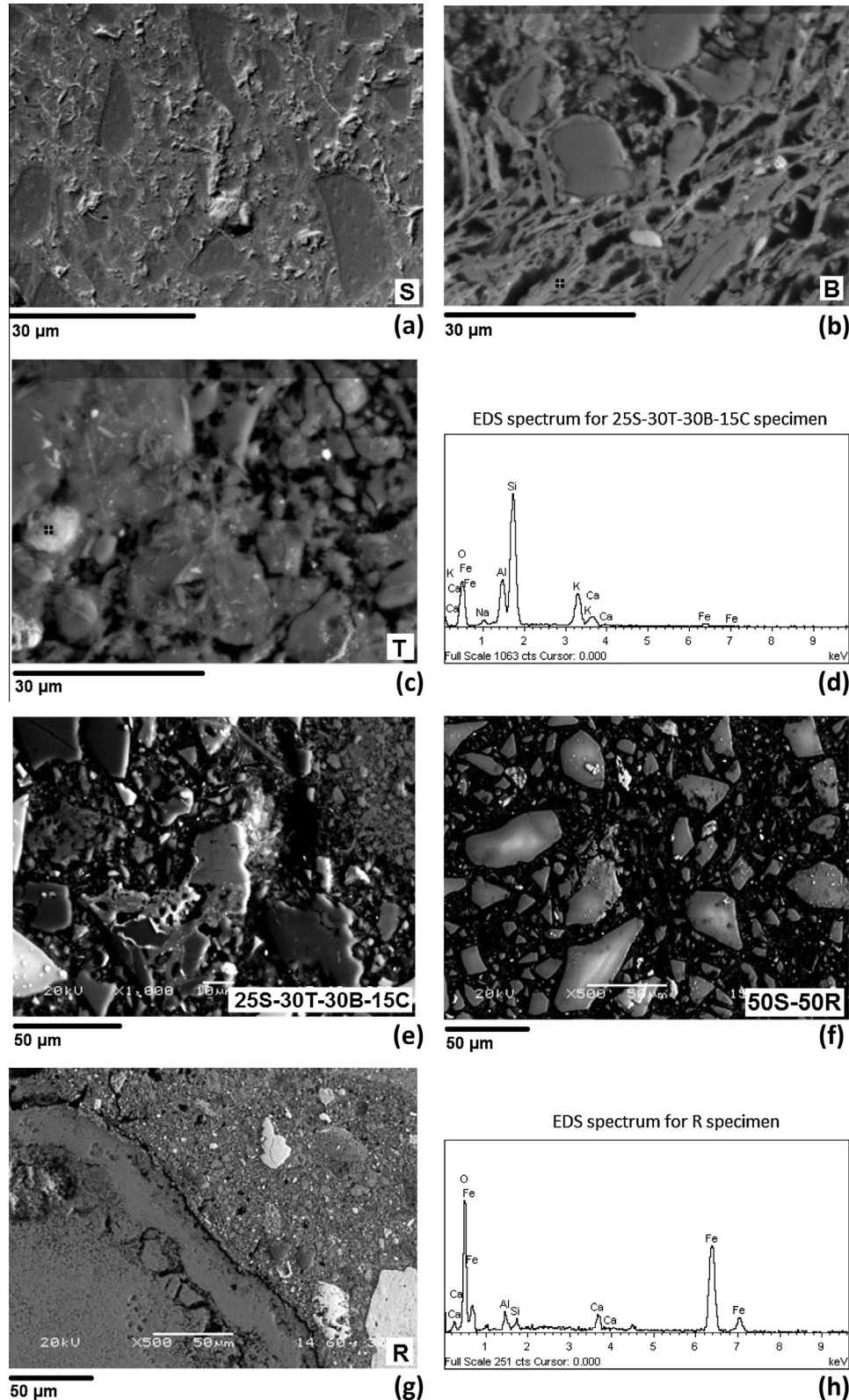

Fig. 7. SEM images and EDS analysis of selected specimens produced from slag, C&D waste components and red mud (specimen codes are presented in Table 3).

heated at 600 °C, compared to the respective non-heated 50S-50R specimen, apart from the fact that the crystallinity of some peaks seems to be slightly reduced.

Fig. 5 presents the TG curves, which denote the % weight loss versus temperature, for the control specimens produced from slag, bricks, tiles and concrete as well as for specimen 25S-30T-30B-15C produced after alkaline activation of a mixture comprising specific percentages of these raw materials with the use of 10 M NaOH. It is shown from this figure that weight is gradually lost for S, T, B and 25S-30T-30B-15C specimens. Up to 200 °C weight loss ranges between 5 and 8% and is due to the loss of free water, while the total weight loss has also a narrow range, between 8 and 13%, indicating that water is bound tightly in the hardened specimens. Therefore, the noticeable strength of these specimens, ranging between 39 and 76 MPa, apart from the favourable mineralogical composition of the raw materials is also due to the appropriate water content present in the initial paste that initiates favourable reactions and results in the formation of a dense structure, $M_n((SiO_2)_z–AlO_2)_n·wH_2O$.

Similar results (not shown) derived for slag-red mud specimens 90S-10R, 80S-20R and 70S-30R, for which the total weight loss varies between 9 and 18% and the acquired strength is high, ranging from 53 to 65 MPa. On the other hand, the control concrete specimen (C) which acquires low compressive strength (7.8 MPa) shows entirely different behaviour. For this specimen, 9% of free water is lost at around 200 °C while the total weight loss, when the temperature reaches 800 °C, increases to 41% due to the partial decomposition of calcite.

Fig. 6 shows the FTIR spectra of selected specimens produced from slag, the components of C&D wastes and red mud, while the respective spectra band assignments are summarized in Table 5. FTIR analysis confirms the presence of the major fingerprints of the aluminosilicate matrix around 1050 cm^{-1} which is more obvious for high strength specimens, namely B, T, S and 25S-30T-30B-15C. These bands are attributed to Si–O stretching vibrations and Si–O–Si or Al–O–Si asymmetric stretching vibrations and their presence indicates higher dissolution of the starting materials, increased amorphicity and thus formation of specimens with high compressive strength, as also discussed in other relevant studies [15,60–62].

The band at 1050 cm^{-1} is also shown, with a lower intensity, for the 50S-50R specimen and the one heated at 600 °C for one hour, indicating that most of the aluminosilicate bonds are not broken during heating at this temperature. A slight shift though of the FTIR spectra to the left implies that several chemical reactions have occurred. On the other hand, for the concrete specimen C that acquires low strength only a small peak at around 1050 cm^{-1} is visible.

The bands at 3440, 2950, 2340 and 1830 cm^{-1} are assigned to stretching and bending H–O–H vibrations of bound water molecules. The bands between 1420 and 1490 cm^{-1} as well as at 880 cm^{-1} are due to atmospheric carbonation and are attributed to the modes of CO_3 in $CaCO_3$. These bands are quite strong in C and 25S-30T-30B-15C specimens. The bands at around 460–710 cm^{-1} which are detected in all specimens are due to in plane Si–O bending and Al–O linkages as well as Si–O–Si and O–Si–O bending vibrations [63,64].

SEM images of selected specimens produced from slag, components of C&D wastes and red mud are shown in Fig. 7. It is seen that the matrix of specimens which acquire the highest compressive strength is homogeneous due to the sufficient dissolution of the raw materials and the formation of aluminosilicate gel (e.g. slag specimen S, Fig. 7a).

The high strength acquired for the B and T specimens, that ranges between 40 and 58 MPa, is due to the development of networks which act as binders between the raw material grains, as

illustrated in Fig. 7b and c, respectively. High content of Si and Al, which are the main elements required for the formation of aluminosilicate bonds, is detected in these specimens. In Fig. 7d an indicative EDS spectrum is shown for specimen 25S-30T-30B-15C (Si and Al are the main elements) for which the SEM image is presented in Fig. 7f.

Finally, a certain degree of homogeneity is shown in 50S-50R specimen (Fig. 7f) where dispersed angular grains of slag are visible. It is mentioned that the matrix of specimen R (Fig. 7g), that is not well solidified and acquires very low strength (2.5 MPa) is quite different; various voids and pores are identified, while almost no gel is formed due to limited alkali activation of red mud grains. In this case Fe is the dominant element, while Si and Al are detected in very small quantities, as deduced from the EDS analysis shown in Fig. 7h.

4. Conclusions

The results of this study show that successful alkali activation of C&D wastes, slag and red mud can be achieved at 80 °C, using NaOH as alkali activator, for the production of construction materials. More specifically, the final products acquire optimum properties only if appropriate ratios of specific mineralogical constituents, namely SiO_2/Al_2O_3 and SiO_2/CaO, are present in the starting mixture, provided of course that sufficient concentration of alkali activator is used. In this case, alkali activation facilitates the formation of Si–O–Si and Al–O–Si bonds and the produced materials obtain beneficial properties. Furthermore, it has been also shown that final products obtained from specific starting mixtures exhibit good thermal behaviour and can be used for fire protection. Another important parameter during alkali activation is the presence of sufficient water in the reactive paste which facilitates early initiation of alkali activation reactions.

The use of analytical techniques provides very useful insights for the characterization and microstructure of the produced specimens. XRD analysis indicates the degree of amorphicity, as well as the presence of partially reacted or unreacted crystalline phases in all specimens. TG analysis shows the presence of tightly bound water in the matrix indicating if specimens will acquire a noticeable strength. FTIR analysis confirms the presence of the major fingerprints of the aluminosilicate alkali activated matrix. SEM analysis shows that the matrix of specimens with improved properties is more homogeneous as a result of the sufficient dissolution of the raw materials used and the formation of aluminosilicate bonds.

References

[1] J. Davidovits, Geopolymers: inorganic polymeric new materials, J. Mater. Educ. 16 (1994) 91–139.

[2] K. Komnitsas, D. Zaharaki, V. Perdikatsis, Effect of synthesis parameters on the compressive strength of low-calcium ferronickel slag inorganic polymers, J. Hazard. Mater. 161 (2009) 760–768.

[3] K. Somna, C. Jaturapitakkul, P. Kajitvichyanukul, P. Chindaprasirt, NaOH activated ground fly ash geopolymer cured at ambient temperature, Fuel 90 (2011) 2118–2124.

[4] M.J.A. Mijarsh, M.A. Megat Johari, Z.A. Ahmad, Synthesis of geopolymer from large amounts of treated palm oil fuel ash: application of the Taguchi method in investigating the main parameters affecting compressive strength, Constr. Build. Mater. 52 (2014) 473–481.

[5] F. Colangelo, R. Cioffi, F. Montagnaro, L. Santoro, Soluble salt removal from MSWI fly ash and its stabilization for safer disposal and recovery as road basement material, Waste Manage. 32 (2012) 1179–1185.

[6] S. Hanjitsuwan, S. Hunpratub, P. Thongbai, S. Maensiri, V. Sata, P. Chindaprasirt, Effects of NaOH concentrations on physical and electrical properties of high calcium fly ash geopolymer paste, Cem. Concr. Compos. 45 (2014) 9–14.

[7] B. Singh, G. Ishwarya, M. Gupta, S.K. Bhattacharyya, Geopolymer concrete: a review of some recent developments, Constr. Build. Mater. 85 (2015) 78–90.

[8] J. Yliniemi, J. Pesonen, M. Tiainen, M. Illikainen, Alkali activation of recovered fuel–biofuel fly ash from fluidised-bed combustion: stabilisation/solidification of heavy metals, Waste Manage. 43 (2015) 273–282.

[9] S.A. Bernal, E.D. Rodríguez, A.P. Kirchheim, J.L. Provis, Management and valorisation of wastes through use in producing alkali-activated cement materials, J. Chem. Technol. Biotechnol. (2016), http://dx.doi.org/10.1002/jctb.4927.

[10] A. Nazer, J. Payá, M.V. Borrachero, J. Monzó, Use of ancient copper slags in Portland cement and alkali activated cement matrices, J. Environ. Manage. 167 (2016) 115–123.

[11] E.I. Diaz, E.N. Allouche, S. Eklund, Factors affecting the suitability of fly ash as source material for geopolymers, Fuel 89 (2010) 992–996.

[12] K. Komnitsas, D. Zaharaki, Geopolymerisation: a review and prospects for the minerals industry, Miner. Eng. 20 (2007) 1261–1277.

[13] S. Ahmari, L. Zhang, Durability and leaching behavior of mine tailings-based geopolymer bricks, Constr. Build. Mater. 44 (2013) 743–750.

[14] K.E. Hafid, M. Hajjaji, Effects of the experimental factors on the microstructure and the properties of cured alkali-activated heated clay, Appl. Clay Sci. 116–117 (2015) 202–210.

[15] D. Rieger, T. Kovářík, J. Říha, R. Medlín, P. Novotnỳ, P. Bělskỳ, J. Kadlec, P. Holba, Effect of thermal treatment on reactivity and mechanical properties of alkali activated shale-slag binder, Constr. Build. Mater. 83 (2015) 26–33.

[16] H. Zhang, V. Kodur, B. Wu, L. Cao, S. Qi, Comparative thermal and mechanical performance of geopolymers derived from metakaolin and fly ash, J. Mater. Civ. Eng. 28 (2) (2016). doi: 10.1061/(ASCE)MT.1943-5533.0001359.

[17] J.C. Swanepoel, C.A. Strydom, Utilisation of fly ash in a geopolymeric material, Appl. Geochem. 17 (8) (2002) 1143–1148.

[18] T. Bakharev, Geopolymeric materials prepared using Class F fly ash and elevated temperature curing, Cem. Concr. Res. 35 (2005) 1224–1232.

[19] J.Z. Xu, Y.L. Zhou, Q. Chang, H.Q. Qu, Study on the factors of affecting the immobilization of heavy metals in fly ash-based geopolymers, Mater. Lett. 60 (6) (2006) 820–822.

[20] Z. Zhang, H. Wang, Y. Zhu, A. Reid, J.L. Provis, F. Bullen, Using fly ash to partially substitute metakaolin in geopolymer synthesis, Appl. Clay Sci. 88–89 (2014) 194–201.

[21] F.U.A. Shaikh, V. Vimonsatit, Compressive strength of fly-ash-based geopolymer concrete at elevated temperatures, Fire Mater. 39 (2) (2015) 174–188.

[22] T.W. Cheng, J.P. Chiu, Fire-resistant geopolymer produced by granulated blast furnace slag, Miner. Eng. 16 (2003) 205–210.

[23] Z. Yunsheng, S. Wei, C. Qianli, C. Lin, Synthesis and heavy metal immobilization behaviors of slag based geopolymers, J. Hazard. Mater. 143 (1–2) (2007) 206–213.

[24] K. Komnitsas, D. Zaharaki, G. Bartzas, Effect of sulphate and nitrate anions on heavy metal immobilisation in ferronickel slag geopolymers, Appl. Clay Sci. 73 (2013) 103–109.

[25] Y. Pontikes, L. Machiels, S. Onisei, L. Pandelaers, D. Geysen, P.T. Jones, B. Blanpain, Slags with a high Al and Fe content as precursors for inorganic polymers, Appl. Clay Sci. 73 (2013) 93–102.

[26] M. Albitar, M.S. Mohamed Ali, P. Visintin, M. Drechsler, Effect of granulated lead smelter slag on strength of fly ash-based geopolymer concrete, Constr. Build. Mater. 83 (2015) 128–135.

[27] M. Salman, Ö. Cizer, Y. Pontikes, R. Snellings, L. Vandewalle, B. Blanpain, K.V. Balen, Cementitious binders from activated stainless steel refining slag and the effect of alkali solutions, J. Hazard. Mater. 286 (2015) 211–219.

[28] J.L. Provis, P. Duxson, J.S.J. Van Deventer, The role of particle technology in developing sustainable construction materials, Adv. Powder Technol. 21 (2007) 2–7.

[29] G. Habert, J.B. D'Espinose De Lacaillerie, N. Roussel, An environmental evaluation of geopolymer based concrete production: reviewing current research trends, J. Clean. Prod. 19 (2011) 1229–1238.

[30] K. Komnitsas, Potential of geopolymer technology towards green buildings and sustainable cities, Procedia Eng. 21 (2011) 1023–1032.

[31] A. Arulrajah, A. Mohammadinia, I. Phummiphan, S. Horpibulsuk, W. Samingthong, Stabilization of recycled demolition aggregates by geopolymers comprising calcium carbide residue, fly ash and slag precursors, Constr. Build. Mater. 114 (2016) 864–873.

[32] W. Hajjaji, S. Andrejkovičová, C. Zanelli, M. Alshaaer, M. Dondi, J.A. Labrincha, F. Rocha, Composition and technological properties of geopolymers based on metakaolin and red mud, Mater. Des. 52 (2013) 648–654.

[33] M. Zhang, T. El-Korchi, G. Zhang, J. Liang, M. Tao, Synthesis factors affecting mechanical properties, microstructure, and chemical composition of red mud-fly ash based geopolymers, Fuel 134 (2014) 315–325.

[34] A. Allahverdi, E.N. Kani, Construction wastes as raw materials for geopolymer binders, Int. J. Civ. Eng. 7 (3) (2009) 154–160.

[35] A. Allahverdi, E.N. Kani, Use of construction and demolition waste (CDW) for alkali-activated or geopolymer cements, in: E. Pacheco-Torgal, V.W.Y. Tam, J.

Labrincha, Y. Ding, J. de Brito (Eds.), Handbook of Recycled Concrete and Demolition Waste, vol. 47, Woodhead Publishing Limited, Cambridge, UK, 2013, pp. 439–475.

[36] S. Ahmari, X. Ren, V. Toufigh, L. Zhang, Production of geopolymeric binder from blended waste concrete powder and fly ash, Constr. Build. Mater. 35 (2012) 718–729.

[37] L. Reig, M.M. Tashima, M.V. Borrachero, J. Monzó, C.R. Cheeseman, J. Payá, Properties and microstructure of alkali-activated red clay brick waste, Constr. Build. Mater. 43 (2013) 98–106.

[38] Z. Sun, H. Cui, H. An, D. Tao, Y. Xu, J. Zhai, Q. Li, Synthesis and thermal behavior of geopolymer-type material from waste ceramic, Constr. Build. Mater. 49 (2013) 281–287.

[39] A. Pathak, S. Kumar, V.K. Jha, Development of building material from geopolymerization of construction and demolition waste (CDW), Trans. Indian Ceram. Soc. 73 (2) (2014) 133–137.

[40] S.R. Zedan, M.R. Mohamed, D.A. Ahmed, A.H. Mohammed, Effect of demolition/construction wastes on the properties of alkali activated slag cement, HBRC J., doi: 10.1016/j.hbrcj.2015.12.001.

[41] K. Komnitsas, D. Zaharaki, A. Vlachou, G. Bartzas, M. Galetakis, Effect of synthesis parameters on the quality of construction and demolition wastes (CDW) geopolymers, Adv. Powder Technol. 26 (2015) 368–376.

[42] Directive 2008/98/EC of the European Parliament and of the Council on waste and repealing certain Directives, Official J. Eur. Union (2008) L.312/3.

[43] F. Pacheco-Torgal, Y. Ding, S. Miraldo, Z. Abdollahnejad, J.A. Labrincha, Are geopolymers more suitable than Portland cement to produce high volume recycled aggregates HPC?, Constr Build. Mater. 36 (2012) 1048–1052.

[44] M. Bravo, J. De Brito, J. Pontes, L. Evangelista, Mechanical performance of concrete made with aggregates from construction and demolition waste recycling plants, J. Clean. Prod. 99 (2015) 59–74.

[45] H. Dahlbo, J. Bachér, K. Lähtinen, T. Jouttijärvi, P. Suoheimo, T. Mattila, S. Sironen, T. Myllymaa, K. Saramäki, Construction and demolition waste management – a holistic evaluation of environmental performance, J. Clean. Prod. 107 (2015) 333–341.

[46] R.V. Silva, J. de Brito, R.K. Dhir, Properties and composition of recycled aggregates from construction and demolition waste suitable for concrete production, Constr. Build. Mater. 65 (2014) 201–217.

[47] P. Duxson, J.L. Provis, G.C. Lukey, S.W. Mallicoat, W.M. Kriven, J.S.J. Van Deventer, Understanding the relationship between geopolymer composition, microstructure and mechanical properties, Colloids Surf. A 269 (2005) 47–58.

[48] H.Y. Leong, D.E.L. Ong, J.G. Sanjayan, A. Nazari, The effect of different Na₂O and K₂O ratios of alkali activator on compressive strength of fly ash based-geopolymer, Constr. Build. Mater. 106 (2016) 500–511.

[49] J.G. Rapazote, C. Laginhas, A. Teixeira-Pinto, Development of building materials through alkaline activation of construction and demolition waste (CDW) – resistance to acid attack, Adv. Sci. Technol. 69 (2010) 156–163.

[50] H. Xu, J.S.J. Van Deventer, G.C. Lukey, Effect of alkali metals on the preferential geopolymerization of stilbite/kaolinite mixtures, Ind. Eng. Chem. Res. 40 (2001) 3749–3756.

[51] K. Komnitsas, D. Zaharaki, V. Perdikatsis, Geopolymerisation of low calcium ferronickel slags, J. Mater. Sci. 42 (2007) 3073–3082.

[52] P.V. Krivenko, G.Yu. Kovalchuk, Directed synthesis of alkaline aluminosilicate minerals in a geocement matrix, J. Mater. Sci. 42 (2007) 2944–2952.

[53] K. Sakkas, P. Nomikos, A. Sofianos, D. Panias, Sodium-based fire resistant geopolymer for passive fire protection, Fire Mater. 39 (3) (2015) 259–270.

[54] Z. Pan, J.G. Sanjayan, B.V. Rangan, An investigation of the mechanisms for strength gain or loss of geopolymer mortar after exposure to elevated temperature, J. Mater. Sci. 44 (7) (2009) 1873–1880.

[55] M. Guerrieri, J.G. Sanjayan, Behavior of combined fly ash/slag-based geopolymers when exposed to high temperatures, Fire Mater. 34 (4) (2010) 163–175.

[56] P.N. Lemougna, K.J.D. MacKenzie, Synthesis and thermal properties of inorganic polymers (geopolymers) for structural and refractory applications from volcanic ash, Ceram. Int. 37 (8) (2011) 3011–3018.

[57] S. Chuah, W.H. Duana, Z. Pan, E. Hunter, A.H. Korayem, X.L. Zhao, F. Collins, J.G. Sanjayan, The properties of fly ash based geopolymer mortars made with dune sand, Mater. Des. 92 (2016) 571–578.

[58] W. Ren, J. Xu, E. Bai, Strength and ultrasonic characteristics of alkali-activated fly ash-slag geopolymer concrete after exposure to elevated temperatures, J. Mater. Civ. Eng. 28 (2) (2016). doi: 10.1061/(ASCE)MT.1943-5533.0001406.

[59] D. Zaharaki, K. Komnitsas, V. Perdikatsis, Use of analytical techniques for identification of inorganic polymer gel composition, J. Mater. Sci. 45 (2010) 2715–2724.

[60] W.K.W. Lee, J.S.J. Van Deventer, The effects of inorganic salt contamination on the strength and durability of geopolymers, Colloid Surf. A 211 (2–3) (2002) 115–126.

[61] J.G.S. Van Jaarsveld, J.S.J. Van Deventer, G.C. Lukey, The effect of composition and temperature on the properties of fly ash- and kaolinite-based geopolymers, Chem. Eng. J. 89 (2002) 63–73.

[62] H.M. Khater, H.A. Abd el Gawaad, Characterization of alkali activated geopolymer mortar doped with MWCNT, Constr. Build. Mater. 102 (2016) 329–337.

[63] G. Socrates, Infrared and Raman Characteristic Group Frequencies, 3rd ed., John Wiley & Sons Ltd, England, 2001.

[64] A. Fernández-Jiménez, A. Palomo, Composition and microstructure of alkali activated fly ash binder: effect of the activator, Cem. Concr. Res. 35 (2005) 1984–1992.